

Origin of excess core loss in amorphous and nanocrystalline soft magnetic materials

H. Huang ¹, H. Tsukahara ^{2,3,*}, A. Kato ^{4,5}, K. Ono ² and K. Suzuki ^{1,†}


¹Department of Materials Science and Engineering, Monash University, Clayton, VIC 3800, Australia

²Department of Applied Physics, Graduate School of Engineering, Osaka University, Suita, Osaka 565-0871, Japan

³Institute of Multidisciplinary Research for Advanced Materials, Tohoku University, Sendai 980-8577, Japan

⁴Toyota Motor Corporation, Mishuku, Susono, Shizuoka 410-1193, Japan

⁵National Institute for Materials Science, Sengen, Tsukuba 305-0047, Japan

 (Received 29 August 2023; revised 26 November 2023; accepted 13 February 2024; published 8 March 2024)

Core losses of amorphous and nanocrystalline soft magnetic ribbons with a range of saturation magnetostriction constants (λ_s) from near zero to $+38 \times 10^{-6}$ have been investigated experimentally with complementary micromagnetic simulations in order to clarify the effect of magnetostriction on the excess loss, i.e., the core loss component unaccounted for by the hysteresis and classical eddy-current losses. The excess loss at 400 Hz and a peak polarization of 1.0 T (P_{ev}) has been found to increase linearly with λ_s , and P_{ev} varies considerably between 0.27 kW/m^3 for near zero-magnetostrictive nc- $\text{Fe}_{85}\text{Nb}_6\text{B}_9$ and 11.0 kW/m^3 for amorphous $\text{Fe}_{80}\text{Si}_{11}\text{B}_9$ with $\lambda_s = +38 \times 10^{-6}$. By substituting the domain wall damping coefficient (β_{dw}) for the eddy current one in Bertotti's statistical model of core losses, the excess loss is predicted to be proportional to $\sqrt{\beta_{dw}}$, indicating that the observed linear increase of P_{ev} is caused by mechanisms where β_{dw} increases with λ_s^2 . Such a quadratic relationship is confirmed by modeling a free wall damping process with lattice anelasticity, suggesting that the anelastic lattice relaxation mediated by magnetostriction could be a potential mechanism. However, the absolute value of β_{dw} remains open because of the uncertainty of the viscosity, and further investigation is needed to validate the mechanism of the excess loss induced by magnetostriction. Our results show that magnetostriction plays a significant role in determining the excess loss in the exchange-softened magnetic materials, and lowering the saturation magnetostriction is crucial for reducing the wall damping effect and the core loss at high frequencies.

DOI: [10.1103/PhysRevB.109.104408](https://doi.org/10.1103/PhysRevB.109.104408)

I. INTRODUCTION

Soft magnetic materials are used as the core part of a range of devices such as transformers and electric motors for magnetic flux multiplication purposes under an alternating-current magnetic field. Since the power loss of these devices can be reduced by lowering the core loss and/or enhancing the saturation magnetic polarization, efficient soft magnetic materials with high saturation magnetization play a significant role in reducing the carbon emission from the utility and transport sectors. The core loss is induced by both static irreversibility and dynamic damping effects on technical magnetization processes. The former is simply governed by the magnetic softness that is reflected in the static coercivity. This loss component is lowered by suppressing the special fluctuation amplitude of the magnetic anisotropy energy (ΔK) by which the domain wall pinning is governed [1,2]. Historically, eddy currents have been regarded as the primary mechanism of the latter in metallic materials such as Fe-Si steels [3]. Thus, much effort has been devoted to increasing the electrical resistance of the core. The intrinsic eddy-current effect can be estimated for a given core geometry. However, for many

soft magnetic materials, this so-called classical eddy-current effect cannot account for the entire dynamic loss component primarily because this classical estimate ignores the additional eddy currents due to the presence of magnetic domains [4–6] or other potential damping effects [7–9]. Thus, the core loss mechanisms are commonly discussed in terms of (i) the hysteresis loss due to static irreversibility, (ii) the classical eddy-current loss, and (iii) the excess loss often referred to as the anomalous loss [10,11].

The excess loss has been studied extensively for metallic sheets and it has commonly been observed that the frequency (f) dependence of the excess loss follows approximately f^n with n around 1.5 [12–15]. This exponent is smaller by 0.5 as compared with that for the classical eddy-current loss. Sakaki and Imagi [12] reported for Si steel cores that the number of domain walls is proportional to $f^{0.4-0.5}$ and explained the exponent around 1.5. Bertotti has developed a series of models [6,13,16,17] to account for eddy-current losses by considering the dynamics of statistically independent magnetic entities composed of interacting domain walls. He considered the frequency dependence of this magnetic microstructure and showed theoretically that the $f^{1.5}$ dependence of the excess loss is attributable to a \sqrt{f} dependence for the number of active domain walls. This \sqrt{f} dependence has been confirmed experimentally for nanocrystalline $\text{Fe}_{73}\text{Cu}_1\text{Nb}_3\text{Si}_{16}\text{B}_7$ by means of the magneto-optical Kerr effect [14]. Although

*Corresponding author: tsukahara@ap.eng.osaka-u.ac.jp

†Corresponding author: kiyonori.suzuki@monash.edu

the frequency dependence of the excess loss is well understood by considering the number of active domain walls, the absolute value of the excess loss may not always be attributable to the extra eddy-current damping effect. For example, the excess loss of amorphous Fe-Si-B alloys could be more than three orders of magnitude greater than the classical eddy-current loss [10]. Such a large extra eddy-current effect may be unlikely and it would be natural to expect other dynamic loss mechanisms in addition to the extra eddy currents due to active domain walls.

It has been reported that the core loss of nanocrystalline $\text{Fe}_{90}\text{Zr}_7\text{B}_3$ at high frequencies is considerably lower than that of amorphous $\text{Fe}_{78}\text{Si}_9\text{B}_{13}$ even though both the hysteresis and classical eddy-current losses are smaller in the latter amorphous alloy [18]. This is due to an exceptionally small excess loss in nanocrystalline $\text{Fe}_{90}\text{Zr}_7\text{B}_3$ and the small magnetostriction of this alloy ($\lambda_s = -1 \times 10^{-6}$) was suggested as a potential reason. The significance of small λ_s for lowering core losses was also suggested earlier by Inomata *et al.* [19] for amorphous Fe-Si-B-Nb alloys. Recently, Tsukahara *et al.* [20] developed a numerical micromagnetic model of nanocrystalline soft magnetic materials where an extra field term due to magnetostriction is considered. This model predicts that the magnetic energy of a moving domain wall dissipates through magnetostriction. These previous reports suggest strongly that λ_s may play an important role in determining the excess loss in soft magnetic materials. Although the effect of magnetostriction on static magnetic softness is well understood by the additional ΔK due to the magnetoelastic anisotropy, the effect of λ_s on the dynamic damping process is insufficiently understood. Moreover, since the domain wall dynamics is highly relevant to spintronic applications [21–24], investigating the domain wall damping induced by magnetostriction is of technological significance. The aim of this paper is to establish the relationship between the excess loss and magnetostriction and thereby demystifying the mechanism of the excess loss in soft magnetic materials. To this end, we have investigated the core losses of a range of nanocrystalline and amorphous alloys where the saturation magnetostriction varies from near zero to as large as $+38 \times 10^{-6}$. Complementary micromagnetic simulations on the effect of magnetostriction on the damping constant of 180° domain walls have also been carried out to confirm the experimental observations.

II. EXPERIMENTAL PROCEDURES

Alloy ingots were prepared by arc melting under a purified Ar atmosphere. The ingots were rapidly solidified by a single-roller melt spinner under an Ar atmosphere, and ribbons with a thickness of 10–25 μm and a width of 10–12 mm were prepared. In addition to the ribbons we prepared, commercially available ribbons of Fe-based amorphous ($\text{Fe}_{80}\text{Si}_9\text{B}_{11}$) and nanocrystalline ($\text{Fe}_{73.5}\text{Cu}_1\text{Nb}_3\text{Si}_{15.5}\text{B}_7$) alloys were also employed in this study. The ribbons were cut into 120-mm-long strips, and also mechanically punched in disks with a diameter of 10 mm and annealed either ultrarapidly for 0.5 s by a pair of preheated Cu blocks or conventionally for 1.8 ks by a tube furnace, both under an Ar atmosphere with no applied magnetic field. The details of the ultrarapid

annealing (URA) are available elsewhere [25]. The annealed ribbon strips were loaded to an Epstein frame to minimize the demagnetization effect. This Epstein frame was used for all the technical magnetization measurements except for the saturation polarization ($J_s = \mu_0 M_s$), which was obtained by a vibrating-sample magnetometer. The coercivity was measured by a dc B - H tracer (Riken BHS-40) and the core loss was measured by an ac B - H analyzer (Iwatsu SY-8219 with a sinusoidal waveform mode). Magnetostriction was measured by a strain gauge slotted in between a pair of annealed disks and adhered to them. The electrical resistivity was measured by a four-point probe method. The mean grain size was estimated by the peak broadening effect of x-ray diffraction acquired on a Bruker D8 Advance diffractometer with $\text{Cu } K\alpha$ radiation.

III. RESULTS AND DISCUSSION

In Table I we list the compositions of alloys investigated along with their thickness (d), density (D_m), mean grain size (D), electrical resistivity (ρ), and magnetic properties. Some of the samples were prepared in our previous reports or commercially produced and some of their properties are adopted from these reports [25–28]. The annealing condition for each sample was determined by measuring the change in the coercivity (H_c) as a function of annealing temperature (T_a) while maintaining the annealing time constant, and T_a resulting in the lowest H_c value was adopted. All the Fe-B binary based alloys require URA for the formation of an exchange-softened nanostructure whereas those alloys containing Nb could be annealed conventionally for obtaining a similar nanostructure. The saturation magnetic polarization of nanocrystalline soft magnetic alloys is known to reflect the mass fraction of ferromagnetic components [29], and alloys free of heavy transition metals tend to exhibit high J_s . The commercial amorphous Fe-Si-B alloy exhibits the highest saturation magnetostriction (λ_s) in the table. The saturation magnetostriction of Fe-based amorphous alloys is known to scale as the square of the spontaneous magnetization [30], and their values are typically around 30 to 40×10^{-6} [31,32], consistent with our result. Contrarily, low λ_s close to zero is obtained for the Nb containing nanocrystalline alloys. This small magnetostriction in the nanostructure has been explained by the negative average value of the nanocrystallites (λ_s^{cr}) and the positive value of the residual amorphous phase (λ_s^{am}) [33]. Since the nanocrystallites and the residual amorphous matrix are exchange coupled, these local contributions are exchange averaged even under total demagnetization. Thus, the saturation magnetostriction constant (λ_s) governing the magnetoelastic effects is determined by

$$\lambda_s = \lambda_s^{\text{cr}} V_{\text{cr}} + \lambda_s^{\text{am}} (1 - V_{\text{cr}}), \quad (1)$$

where V_{cr} is the volume fraction of the crystalline phase. Although the magnetostriction of nanocrystalline alloys is lower than that of the amorphous alloy, a marked increase in λ_s is seen when Co is added to Fe-based nanocrystalline alloys because both λ_s^{cr} and λ_s^{am} are increased dramatically by Co addition [27]. Thus, soft magnetic ribbons with a wide range of λ_s values between ~ 0 and $+38 \times 10^{-6}$ are obtained.

Figure 1 shows the change in the core loss (P_m) as a function of the maximum magnetic polarization (J_m) for all

TABLE I. Nanocrystalline and amorphous alloys investigated along with their mean grain size (D), density (D_m), thickness (d), saturation polarization (J_s), remanent polarization (J_r), coercivity (H_c), electrical resistivity (ρ), and saturation magnetostriction (λ_s). The ribbon samples were annealed ultrarapidly (URA) or conventionally (CA).

Alloy	Annealing Condition	D (nm)	D_m (10^3 kg/m 3)	d (μ m)	J_s (T)	J_r/J_s	H_c (A/m)	ρ ($\mu\Omega$ m)	λ_s (10^{-6})
Fe $_{87}$ B $_{13}$	URA, 773 K for 0.5 s	16	7.62	13.0	1.92	0.42	6.4	0.62	12
Fe $_{86}$ B $_{13}$ Cu $_1$	URA, 773 K for 0.5 s	14	7.63	12.3	1.89	0.30	3.5	0.58	13
(Fe $_{0.8}$ Co $_{0.2}$) $_{86}$ B $_{14}$	URA, 763 K for 0.5 s	22	7.76	14.4	2.00	0.44	8.0	0.65	24
(Fe $_{0.75}$ Co $_{0.25}$) $_{87}$ B $_{13}$	URA, 763 K for 0.5 s	20	7.82	14.0	2.04	0.47	10.0	0.51	30
(Fe $_{0.99}$ Co $_{0.01}$) $_{86}$ B $_{13}$ Cu $_1$	URA, 763 K for 0.5 s	15	7.63	15.2	1.90	0.31	11.6	0.58	14
(Fe $_{0.98}$ Co $_{0.02}$) $_{86}$ B $_{13}$ Cu $_1$	URA, 763 K for 0.5 s	15	7.64	13.8	1.91	0.28	11.0	0.60	15
Fe $_{85}$ Nb $_6$ B $_9$	CA, 898 K for 1.8 ks	11	7.85	12.7	1.67	0.38	5.8	0.51	~ 0
Fe $_{82}$ Nb $_6$ B $_{12}$	CA, 898 K for 1.8 ks	11	7.78	20.0	1.53	0.35	8.0	0.56	1.7
Fe $_{80}$ Nb $_6$ B $_{14}$	CA, 898 K for 1.8 ks	10	7.75	25.9	1.50	0.38	4.2	0.63	2.5
Fe $_{73.5}$ Cu $_1$ Nb $_3$ Si $_{15.5}$ B $_7$	CA, 843 K for 1.8 ks	13	7.35	19.2	1.23	0.40	1.6	1.15	0.5
Fe $_{80}$ Si $_9$ B $_{11}$	CA, 623 K for 7.2 ks		7.20	23.5	1.56	0.44	2.3	1.32	38

the alloys listed in Table I. The $P_m - J_m$ curves were acquired at frequencies between 10 Hz and 30 kHz and the results at 50 Hz, 400 Hz, 1 kHz, and 10 kHz are shown as examples. Both nanocrystalline Fe $_{85}$ Nb $_6$ B $_9$ and Fe $_{73.5}$ Cu $_1$ Nb $_3$ Si $_{15.5}$ B $_7$ consistently show the lowest P_m values at all the measurement conditions except the J_m range near saturation. These two samples exhibit the smallest λ_s ($< 10^{-6}$) among the

samples investigated, showing that the saturation magnetostriction plays an important role in the dynamic loss mechanism.

As mentioned briefly above, the core loss mechanisms have traditionally been discussed by assuming at least the three components, namely, the hysteresis loss (P_h), the classical eddy-current loss (P_c), and the excess loss (P_e). Hence, the measured core loss (P_m) is expressed by

$$P_m = P_h + P_c + P_e. \quad (2)$$

The classical eddy-current loss is obtained by solving Maxwell's equations for a sheet geometry and under a sinusoidally modulated magnetic induction [6]. The following solution is relevant to our samples:

$$P_c = \frac{(\pi d f B_m)^2}{6 \rho D_m}, \quad (3)$$

where D_m is the density and B_m is the peak induction, which is approximated by J_m in the present study. This solution reflects the relationship where the classical eddy-current dissipation is proportional to $(dB/dt)^2$. The excess loss corresponds to the loss component that cannot be attributed to $P_h + P_c$ and thus, the mechanism of P_e could be open to any dynamic origins including the extra eddy currents in the vicinity of active domain walls.

In Fig. 2 we show some typical examples of the measured $J-H$ curves at $J_m = 1$ T and $f = 1, 5,$ and 10 kHz for samples with small (~ 0 for nanocrystalline Fe $_{85}$ Nb $_6$ B $_9$), medium ($+13 \times 10^{-6}$ for nanocrystalline Fe $_{86}$ B $_{13}$ Cu $_1$), and large ($+38 \times 10^{-6}$ for amorphous Fe $_{80}$ B $_9$ Si $_{11}$) λ_s values. In each ac hysteresis plot, the dc hysteresis curve with $J_m = 1$ T and the calculated shift in H due to the classical eddy current are also shown in order to indicate the hysteresis loss (W_h) and the classical eddy-current loss (W_c) per hysteresis cycle. The residue outside the $W_h + W_c$ area corresponds to the excess loss (W_e). Owing to the high electrical resistivity and small sample thickness of these amorphous and nanocrystalline ribbons, the classical eddy-current loss remains only a minor loss component in all the samples regardless of the measurement conditions. However, the excess loss behavior differs remarkably between these samples. The excess loss in

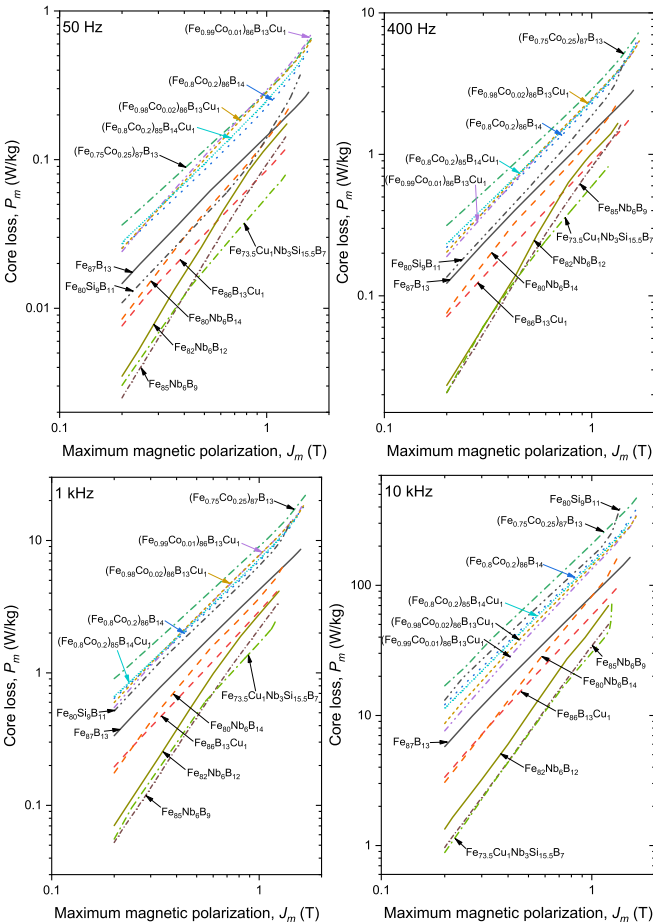


FIG. 1. Change in core loss as a function of the maximum polarization (J_m) at 50 Hz, 400 Hz, 1 kHz, and 10 kHz.

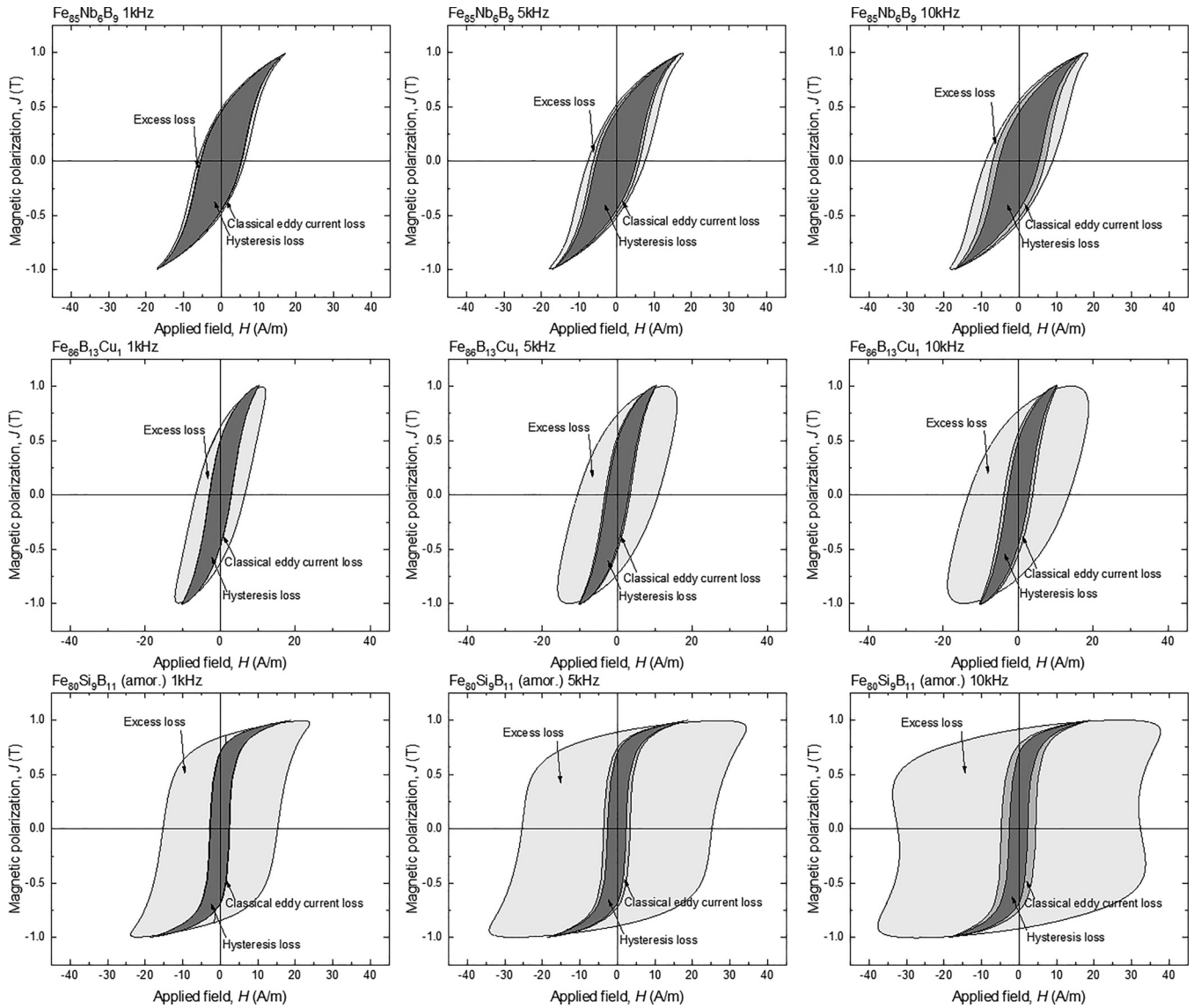


FIG. 2. J - H loops of nanocrystalline $\text{Fe}_{85}\text{Nb}_6\text{B}_9$ ($\lambda_s \sim 0$), $\text{Fe}_{86}\text{B}_{13}\text{Cu}_1$ ($\lambda_s = 13 \times 10^{-6}$), and amorphous $\text{Fe}_{80}\text{Si}_9\text{B}_{11}$ ($\lambda_s = 38 \times 10^{-6}$) acquired at 1, 5, and 10 kHz with a peak polarization (J_m) of 1.0 T. The curves obtained under a pseudostatic condition (~ 0.1 Hz) with the same J_m (annotated by hysteresis loss) along with the shift of H due to the classical eddy-current effect are also shown.

the near zero-magnetostrictive $\text{Fe}_{85}\text{Nb}_6\text{B}_9$ is the smallest in these samples and remains a minor loss component even at higher frequencies. Contrarily, the excess loss is by far the largest loss component in amorphous $\text{Fe}_{80}\text{Si}_9\text{B}_{11}$ where the magnetostriction is the largest ($+38 \times 10^{-6}$). The $\text{Fe}_{86}\text{B}_{13}\text{Cu}_1$ alloy with a medium λ_s of 13×10^{-6} exhibits a moderate contribution of the excess loss. The low core losses observed for the near zero-magnetostrictive $\text{Fe}_{85}\text{Nb}_6\text{B}_9$ is readily understood by the exceptionally small excess loss. The effect of λ_s on magnetic softness has often been argued by considering the magnetoelastic anisotropy [1,2]. However, this simple pseudostatic argument has limited relevancy to our results as the correlation between H_c and λ_s is poor in the present study presumably because the variation of ΔK between samples reflects $\langle K_1 \rangle$. Rather, the significance of λ_s lies in its influence on the dynamic technical magnetization processes.

The extent of the excess loss is often discussed by taking the ratio of the excess loss to the classical eddy-current loss;

this ratio plus 1 is commonly referred to as the anomaly factor [3]. Although this factor is sound when the origin of the excess loss is due to extra eddy-current effects, it could be misleading when the damping mechanism is unrelated to eddy currents. The anomaly factor tends to be large in ribbon-shaped alloys and very large values around 10 [3] were reported for amorphous $\text{Fe}_{80}\text{B}_{20}$ and $\text{Fe}_{40}\text{Ni}_{40}\text{B}_{20}$ alloys at 20 Hz [10]. However, these enormous values were due to the small classical eddy-current loss, and the anomaly factor does not always reflect the absolute value of the excess loss. Hence, we compare the absolute value of the excess loss here. The excess loss was extracted from the results in Fig. 1 by subtracting P_h and P_c , and some examples are plotted in Fig. 3. In this figure, the excess loss is shown as a function of the product of maximum magnetic polarization and frequency ($J_m f$), which reflects dJ/dt . We limit the J_m range between 0.4 and 1.0 T for these plots in order to avoid the instantaneous increase of dJ/dt near the technical saturation. The plot for each alloy

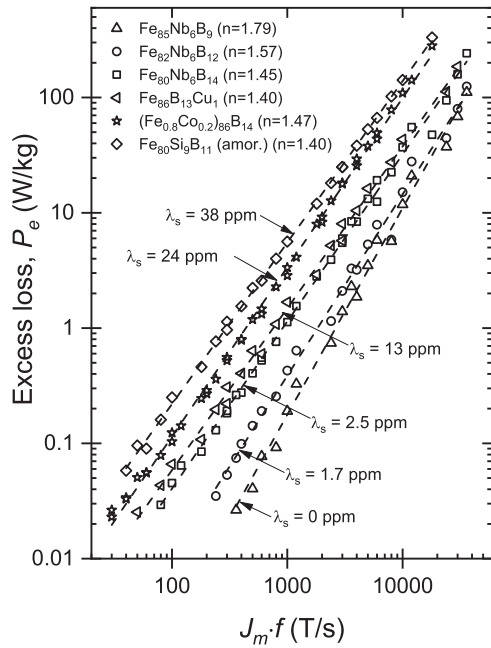


FIG. 3. The change in the excess loss (P_e) as a function of $J_m f$ for alloys with the saturation magnetostriction (λ_s) ranging from near zero to 38×10^{-6} .

follows $(J_m f)^n$ dependence with n between 1.40 and 1.79. This behavior is close to the well-known $(J_m f)^{1.5}$ dependence [6,12], suggesting that the number of active domain walls in our samples follows approximately a $\sqrt{dJ/dt}$ dependence. The excess loss of the ribbon samples studied here varies more than an order of magnitude and the value appears to depend highly on the saturation magnetostriction.

In Fig. 4 we show the relationship between λ_s and the excess loss at $f = 400$ Hz and $J_m = 1$ T, a condition commonly used for evaluating the core losses in materials used in electric motors. In this figure, the excess loss (P_{ev}) is given in the volumetric power density. Strikingly, P_{ev} increases approximately linearly from 0.27 to 11.0 kW/m^3 with increasing λ_s from ≈ 0 to $+38 \times 10^{-6}$, indicating explicitly that magnetostriction plays a significant role in determining the excess loss in the exchange-softened ribbons investigated. At 400 Hz and under the peak polarization well below saturation, the technical process is primarily caused by the displacement of the domain walls. The excess eddy-current loss under this technical process is known to be pronounced when the 180° domain walls are aligned parallel to the applied field direction, i.e., a high squareness case. Fiorillo and Beatrice [34] studied the core loss of a near zero-magnetostrictive $\text{Co}_{67}\text{Fe}_4\text{B}_{14.5}\text{Si}_{14.5}$ amorphous alloy with $J_m = 0.05$ T. They have found that the core loss varies by more than an order of magnitude by changing the squareness. Judging by their results for the high squareness ribbon, the excess loss is estimated to be $\sim 3 \text{ kW/m}^3$ at 8 kHz ($J_m f = 400$), comparable to the P_{ev} values of nc- $\text{Fe}_{80}\text{Nb}_6\text{B}_{14}$ and nc- $\text{Fe}_{86}\text{B}_{13}\text{Cu}_1$ with $\lambda_s = 2.5$ to 13×10^{-6} . Hence, the excess loss can be substantial even if $\lambda_s = 0$ when J_r/J_s is high because of the large excess eddy-current effect [34]. However, no apparent effect of λ_s on the squareness is evident in our experiments; J_r/J_s of our ribbons

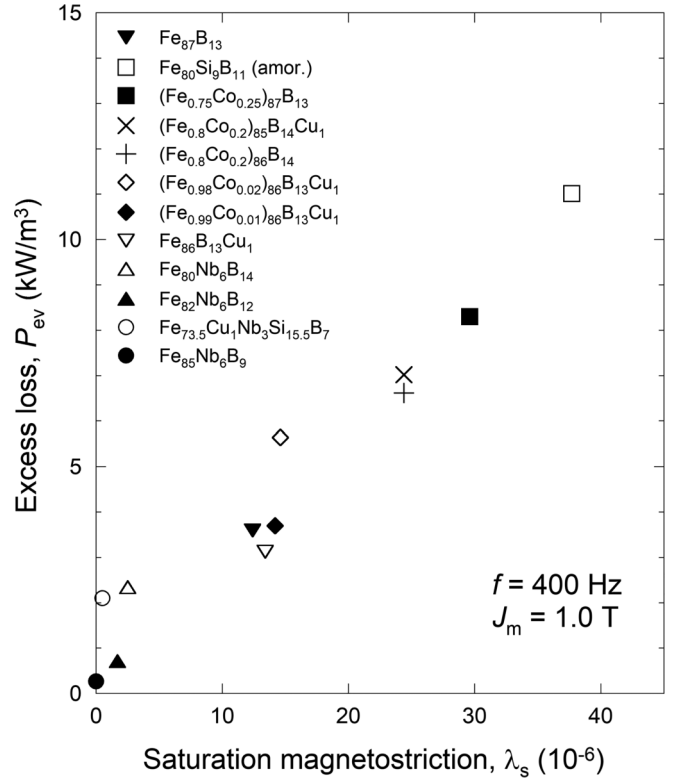


FIG. 4. Relationship between the excess loss (P_{ev} in W/m^3) and the saturation magnetostriction (λ_s).

in Table I fluctuates around 0.4. Thus, such a lossy domain configuration is unlikely in our samples.

The excess loss in near zero-magnetostrictive ribbons has also been investigated for nanocrystalline $\text{Fe}_{73}\text{Cu}_1\text{Nb}_3\text{Si}_{16}\text{B}_7$ by Flohrer *et al.* [35]. They investigated the dynamic domain configurations and the core losses of nc- $\text{Fe}_{73}\text{Cu}_1\text{Nb}_3\text{Si}_{16}\text{B}_7$ toroidal cores with induced magnetic anisotropy (K_u) where the easy axis is induced along the circumference of the toroid. The peak induction used was 1.14 T. They have found that the number of active domain walls is reduced by K_u and the excess eddy-current loss is increased. The largest excess loss observed for nc- $\text{Fe}_{73}\text{Cu}_1\text{Nb}_3\text{Si}_{16}\text{B}_7$ with the strongest K_u was about $3\text{--}4 \text{ kW/m}^3$ at $J_m f = 400$, similar to the corresponding value reported for the a- $\text{Co}_{67}\text{Fe}_4\text{B}_{14.5}\text{Si}_{14.5}$ ribbon with longitudinal K_u [34]. This confirms the potential significance of the excess eddy-current effect in near zero-magnetostrictive ribbons. Thus, the linear increase of P_{ev} seen in Fig. 4 might be attributed to the effect of magnetoelastic K_u on the excess eddy-current loss through the reduction of the number of domain walls. However, this effect seems to be limited in our ribbons. Assuming the typical residual stress in stress-relieved ribbons (a few MPa) [35], the magnetoelastic anisotropy in our samples is at most $\sim 100 \text{ J/m}^3$ even if we adopt the largest λ_s ($+38 \times 10^{-6}$). However, this energy density is comparable to the typical annealing-induced K_u in nc-Fe-Nb-B [36] and nc-Fe-B-(Cu) [29] alloys, which is manifested in their D^3 dependence of H_c . Thus, the variation of λ_s hardly causes a significant change in K_u in our nanocrystalline ribbons. Moreover, the wall energy is proportional to the square root of the anisotropy energy and the domain

size is governed by the square root of the wall energy [2]. Consequently, the magnetoelastic K_u fails to explain the linear scaling between P_e and λ_s .

The discussion above suggests that we may need to explore the wall damping mechanisms beyond eddy-current models. The motions of a 180° domain wall are described by the following well-known relationship:

$$m\ddot{q} + \beta_{dw}\dot{q} + kq = 2J_s H_{ext}, \quad (4)$$

where q is the center position of the domain wall, m is the effective mass of the domain wall, k is spring constant, and H_{ext} is the external magnetic field. The energy dissipation due to spin damping is governed by $\beta_{dw} = (2J_s/\mu_0\gamma\delta_w)\alpha$, where δ_w is the domain wall width and α is the Gilbert damping constant. Fiorillo *et al.* [9,37] have explained the excess loss in ferrites by extending Bertotti's statistical model of core losses [6] to insulators where eddy currents are negligible. They assumed that spin damping, instead of the eddy-current damping, is the leading loss mechanism and have shown that the model can describe the frequency dependence of core losses due to the wall damping up to about 100 kHz, the threshold of the rotation process. According to their report [37], the excess loss (in W/m^3) is expressed by

$$P_{ev} \cong 4\sqrt{\beta L J_s V_0} [(J_m/J_s) f]^{3/2}, \quad (5)$$

where L is the ribbon length, and the damping coefficient β is β_{dw} or β_{eddy} depending on the governing mechanism. The damping coefficient due to the eddy current β_{eddy} is written as $4\sigma G J_s^2 d$ where σ is conductivity, $G = 0.1356$, and d is the ribbon thickness. Since the ribbon cross-sectional area S is Ld , this equation reproduces the original Bertotti model [17] for $\beta = \beta_{eddy}$, i.e.,

$$P_{ev} \cong 8\sqrt{\sigma G S V_0} (J_m f)^{3/2}, \quad (6)$$

where V_0 is a phenomenological parameter with a dimension of A/m.

Since the excess loss in Eq. (5) is proportional to $\sqrt{\beta}$, potential dissipation processes must satisfy a relation of $\beta \propto \lambda_s^2$ to account for the linear dependence of P_{ev} on λ_s . Peria *et al.* [38] investigated the heating rate due to Gilbert damping in magnetostrictive $Fe_{70}Ga_{30}$ films and explained the effect of magnetostriction based on the damping of phonon modes [39]. Peria *et al.* obtained the Gilbert damping constant due to magnetostriction (α_{me}) as $\alpha_{me} = (4\mu_0\gamma/J_s)\eta\lambda^2$, where η is the viscosity and $\lambda = \lambda_s$ for the exchange-coupled systems. Thus, the damping coefficient is expected to be proportional to the square of λ_s . Still, it remains unclear whether or not this model is applicable to the damping of the 180° domain wall motion because their discussion is limited to shear strains in small coherent oscillation of the magnetization. In the following, we will clarify the relationship between magnetostriction and the damping parameter for the domain wall motion by simulating free-damping oscillation of the 180° domain wall.

The effect of magnetostriction on β_{dw} can be calculated by using a micromagnetic simulation code developed recently by Tsukahara *et al.* [20] who considered an additional field term due to the local magnetostriction on top of the field terms in the Landau–Lifshitz–Gilbert equation. In this code,

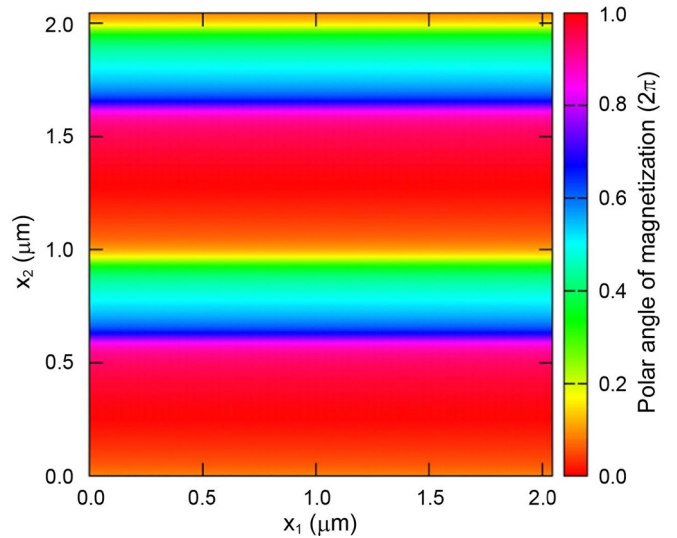


FIG. 5. Initial magnetization state of micromagnetic simulations. Colors show polar angles of magnetization in the x_1x_2 plane. Domain walls are displaced from relaxed position. Magnetic polarization of the initial state is 0.7 T. Animated simulation results can be found in the Supplemental Material [40].

both the elastic and the magnetoelastic energy densities are considered along with the time-dependent evolution of lattice strain due to anelasticity. Thus, the model describes the dissipation of the magnetic energy in moving domain walls due to the anelastic relaxation induced by magnetostriction. We simulated the free-damping behaviors of simple 180° domain walls using the code [20] for a single-crystalline thin film where the magnetostriction is isotropic ($\lambda_{100} = \lambda_{111} = \lambda_s$). A simulation model of $2048 \times 2048 \times 2$ nm³ is discretized into calculation cells of $2 \times 2 \times 2$ nm³. Except for the magnetocrystalline anisotropy (K_1), magnetostriction constants, and electrical conductivity (σ), we adopted the material parameters of α -Fe. Figure 5 shows the initial magnetization state of the micromagnetic simulations for the free-damping oscillation of the domain walls. The simulation model has four stripe domains where the edge is aligned parallel to the crystal axis of α -Fe. The external magnetic field displaced the domain wall position by 82.2 nm from the relax position and this displacement of the domain wall causes a magnetic polarization of 0.7 T. This polarization raises the dipole energy which generates restoring forces acting on the domain walls. After polarizing the system, we removed the external magnetic field and simulated oscillations of the magnetic domain walls. To isolate the effects of magnetostriction from other influential parameters, σ , K_1 , and the Gilbert damping constant were omitted. The model used is free of defects that inhibit the domain wall oscillation. Hence, the damping of the domain wall oscillation represents solely the energy dissipation due to magnetostriction. The details of the domain wall oscillation are shown in the Supplemental Material [40], which contains an animation of magnetization dynamics for $\lambda_s = 4.0 \times 10^{-5}$. The four domain walls oscillate coherently and the oscillation amplitude decreases gradually due to magnetostriction.

The damping constant due to magnetostriction can be estimated by using an analytical equation of free-damping

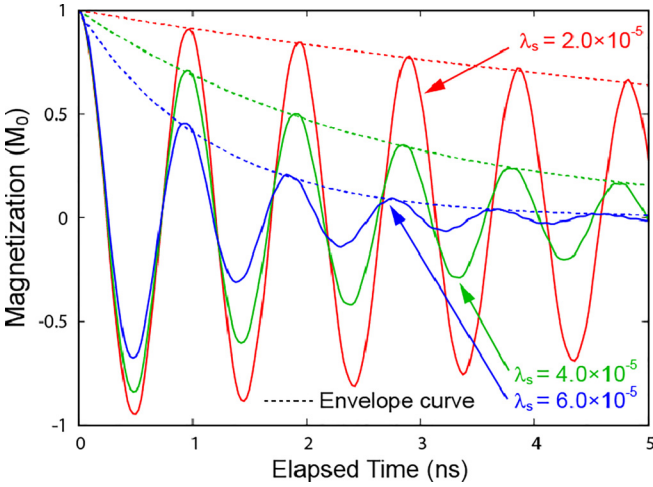


FIG. 6. Micromagnetically simulated free-damping process of 180° domain walls for a range of saturation magnetostriction (λ_s). Solid lines are the magnetization oscillations and dotted lines are envelope curves.

oscillation, i.e., the oscillation of the domain wall when the external magnetic field is absent. In this case, the relevant equation for the domain wall motion becomes

$$\ddot{q} + 2\kappa\dot{q} + \omega_0^2q = 0, \quad (7)$$

where κ is the damping parameter, $\kappa = \beta_{dw}/2m$, and ω_0 is the eigenfrequency of the domain wall oscillation, $\omega_0 = \sqrt{k/m}$. After a straightforward calculation, one obtains the following solution:

$$q = q_0 e^{-\kappa t} \cos(\omega_d t + \phi), \quad (8)$$

where q_0 and ϕ are arbitrary constants and $\omega_d = \sqrt{\omega_0^2 - \kappa^2}$. The magnetization of the magnetic material is also oscillated due to the domain wall displacement. When the relation between the changes in the magnetization ΔM and the domain wall displacement Δq is expressed by $\Delta M = v_{dw}\Delta q$, the damping oscillation of the magnetization is written by

$$M(t) = M_0 e^{-\zeta\omega_0 t} \cos(\omega_d t + \phi), \quad (9)$$

where $M_0 = v_{dw}q_0$, and $\zeta = \beta_{dw}/2\sqrt{mk}$ is the dimensionless damping parameter, which we can estimate using the simulation results. Figure 6 shows examples of the simulation results where the change in magnetization is plotted as a function of time for $\lambda_s = 2, 4,$ and 6×10^{-5} . Each curve follows a typical free-damping behavior as expressed by Eq. (9). In this simulation model, $\omega_0 = 1.03$ GHz was obtained by the simulation for $\lambda_s = 0$. The damping of the magnetization oscillation increases with increasing magnetostriction constant. The dimensionless damping parameter ζ was obtained by calculating the envelope curve of the simulation results for a range of λ_s values. The obtained coefficient is plotted against λ_s in Fig. 7 where ζ appears to be proportional to approximately the square of λ_s . Consequently, as far as the scaling is concerned, the dependence of the excess loss on the saturation magnetostriction in our ribbons is attributable to the anelastic relaxation via magnetostriction.

Since the eddy current also contributes to the excess loss, it is important to estimate typical values of β_{eddy} and compare

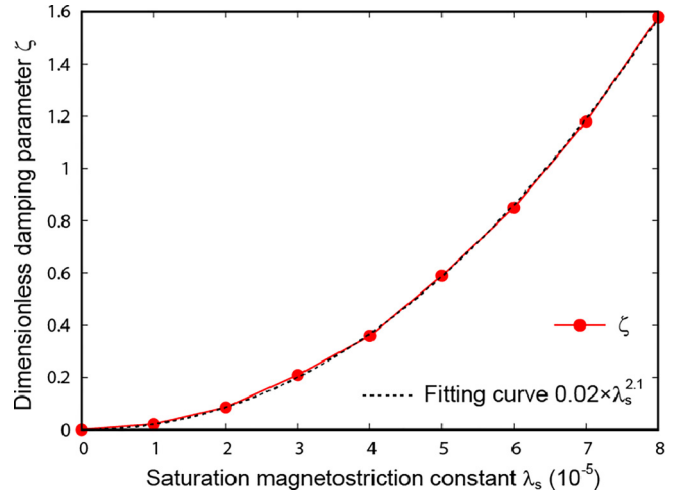


FIG. 7. Dimensionless damping parameter ζ extracted from the micromagnetically simulated free-damping process. ζ is estimated by using the envelope curves of the free-damping oscillation of the magnetization. Dotted line represents a regression curve ($\zeta = 0.02 \times \lambda_s^{2.1}$) obtained by least-squares fitting.

it with β_{dw} . We estimate β_{eddy} for nc-(Fe_{0.8}Co_{0.2})₈₆B₁₄ as the excess loss of this alloy follows almost the ideal $f^{1.5}$ power dependence. Adopting the material parameters in Table I, β_{eddy} is estimated as 48 kg/(s m²). To estimate β_{dw} , the values of the domain wall width and the viscosity (η) are indispensable. The domain wall width ($\delta_w = \pi\sqrt{A/(K)}$) for nc-(Fe_{0.8}Co_{0.2})₈₆B₁₄ is estimated to be $\approx 4 \times 10^{-7}$ m using the exchange stiffness ($A = 3.1 \pm 0.1$ pJ/m) [41] reported for nc-Fe₈₉Zr₇B₃Cu₁, and adopting the induced anisotropy of nc-(Fe_{0.8}Co_{0.2})₉₀Zr₇B₃ ($K_u \approx 220$ J/m³) [42] for $\langle K \rangle$. The η values of solid metals in the literature [43] are often contradictory and the experimental results for Fe-based alloys vary over two orders of magnitude between 10^3 and 10^5 Pa s. If we assume $\eta = 10^4$, the damping coefficient β_{dw} is estimated as 116 kg/(s m²), larger than β_{eddy} . These estimates suggest the possibility that the energy dissipation of the domain wall motion is governed by β_{dw} due to magnetostriction, although we cannot unequivocally conclude the dominance of β_{dw} without an accurate estimate of the viscosity.

In addition to the uncertainty of the viscosity, the Gilbert damping constant (α) estimated from the wall damping coefficient is orders of magnitude larger than the typical α values obtained by ferromagnetic resonance (FMR). In the above estimate of β_{dw} (116 kg s⁻¹ m⁻²) the equivalent Gilbert damping constant becomes as large as 2.6. It is worth mentioning here that large values of α are also expected for the wall damping process due to the excess eddy current in alloy ribbons with exceptionally low losses. For example, β_{eddy} for nc-Fe_{73.5}Cu₁Nb₃Si_{15.5}B₇ is estimated to be ≈ 14 kg/(s m²) with the J_s , ρ , and d values in Table I. This β_{eddy} is equivalent to α at least above 1 if we adopt $\delta_w \sim 10^{-6}$ m [44], implying that the eddy-current damping could be considerable. A possible explanation for the discrepancy in the Gilbert damping constant is the frequency (~ 10 GHz) used for FMR. In such a high frequency, the domain wall process is relaxed and the observable damping constant may not reflect the wall damping

process active in a kilohertz range. Still, because of these unsettled parameters (i.e., α and η) the absolute value of β_{dw} due to the anelastic lattice relaxation remains open and further investigation is needed to validate the potential mechanism of the anelastic lattice relaxation mediated by magnetostriction.

IV. CONCLUSION

The core losses of amorphous and nanocrystalline soft magnetic alloys with a range of saturation magnetostriction constants (λ_s) between near zero and $+38 \times 10^{-6}$ have been investigated in order to clarify the origin of excess core loss in soft magnetic materials. The core loss was measured in a frequency (f) range from 10 Hz to 30 kHz with the maximum magnetic polarization (J_m) from 0.2 T to near saturation of each sample. The measured loss was separated into the hysteresis, classical eddy current, and excess losses. The excess loss under $J_m = 0.4$ and 1.0 T and $f = 10$ Hz to 30 kHz follows $(J_m f)^n$ dependence with n around 1.5, implying that the number of active domain walls in our samples changes approximately as $\sqrt{dJ/d\dot{f}}$. The excess loss increases as large as 40-fold from 0.27 to 11.0 kW/m³ with an increase in λ_s from ≈ 0 to $+38 \times 10^{-6}$, indicating a strong effect of the saturation magnetostriction in determining the excess loss. Owing to the near zero-magnetostriction, nc-Fe₈₅Nb₆B₉ exhibits one of the lowest core loss values next to the ultrasoft nc-Fe_{73.5}Cu₁Nb₃Si_{15.5}B₇ with $\lambda_s \approx +0.5 \times 10^{-6}$. Our micro-magnetic simulations on the free-damping process of 180° domain walls predicts that the wall damping coefficient (β_{dw})

is proportional to λ_s^2 . Adopting Bertotti's statistical model of core losses with β_{dw} , the excess loss is predicted to be proportional to $\sqrt{\beta_{dw}}$, supporting the linear correlation between the excess loss and λ_s . However, the absolute value of β_{dw} due to magnetostriction remains open because of the uncertainty of the viscosity and the model validity requires further investigation. Although the magnetoelastic anisotropy is known to be a hindrance to the wall displacement, this conventional pseudostatic model has limited relevance to our results as the effect of λ_s on static coercivity is limited. Rather, the significance of magnetostriction lies in its effect on the dynamic domain wall damping, which governs the excess core loss at high frequencies. For nanocrystalline soft magnetic materials, simply aiming at small coercivity by grain refinement is insufficient and one must focus also on suppressing the saturation magnetostriction.

ACKNOWLEDGMENTS

This work is supported financially by the Australian Research Council (Grant No. LP190100294). H.H. and K.S. acknowledge the use of facilities within the Monash X-ray Platform. Some of the ribbon samples were prepared by Dr. R. Parsons for our previous reports. The amorphous Fe_{73.5}Cu₁Nb₃Si_{15.5}B₇ and Fe₈₀Si₉B₁₁ ribbons were provided by Dr. G. Herzer and Dr. N. Ito, respectively, and K.S. is thankful for their support. H.H. is grateful to Monash University for the financial support through its postgraduate scholarship schemes.

-
- [1] R. M. Bozorth, *Ferromagnetism* (Wiley, Hoboken, 2003).
- [2] S. Chikazumi, *Physics of Ferromagnetism* (Oxford University Press, Oxford, 1997).
- [3] B. D. Cullity, *Introduction to Magnetic Materials* (Addison-Wesley, Reading, 1972), p. 493.
- [4] H. J. Williams, W. Shockley, and C. Kittel, Studies of the propagation velocity of a ferromagnetic domain boundary, *Phys. Rev.* **80**, 1090 (1950).
- [5] R. H. Pry and C. P. Bean, Calculation of the energy loss in magnetic sheet materials using a domain model, *J. Appl. Phys.* **29**, 532 (1958).
- [6] G. Bertotti, *Hysteresis in Magnetism* (Academic Press, San Diego, 1998), p. 391.
- [7] D. C. Jiles, Frequency dependence of hysteresis curves in 'non-conducting' magnetic materials, *IEEE Trans. Magn.* **29**, 3490 (1993).
- [8] H. Suhl, Theory of the magnetic damping constant, *IEEE Trans. Magn.* **34**, 1834 (1998).
- [9] F. Fiorillo, M. Coisson, C. Beatrice, and M. Pasquale, Permeability and losses in ferrites from dc to the microwave regime, *J. Appl. Phys.* **105**, 07A517 (2009).
- [10] M. G. Blundell, C. D. Graham, Jr., and K. J. Overshott, Variation of power loss of amorphous ribbon alloys with frequency and applied stress, *J. Magn. Mater.* **19**, 174 (1980).
- [11] H. Fujimori, H. Yoshimoto, T. Masumoto, and T. Mitera, Anomalous eddy current loss and amorphous magnetic materials with low core loss, *J. Appl. Phys.* **52**, 1893 (1981).
- [12] Y. Sakaki and S. Imagi, Relationship among eddy current loss, frequency, maximum flux density and a new parameter concerning the number of domain walls in polycrystalline and amorphous soft magnetic materials, *IEEE Trans. Magn.* **17**, 1478 (1981).
- [13] G. Bertotti, Space-time correlation properties of the magnetization process and eddy current losses: Applications. II. Large wall spacing, *J. Appl. Phys.* **55**, 4348 (1984).
- [14] S. Flohrer, R. Schäfer, J. McCord, S. Roth, L. Schultz, F. Fiorillo, W. Günther, and G. Herzer, Dynamic magnetization process of nanocrystalline tape wound cores with transverse field-induced anisotropy, *Acta Mater.* **54**, 4693 (2006).
- [15] H. Huang, R. Parsons, H. Tsukahara, M. Yano, T. Shoji, A. Kato, K. Ono, and K. Suzuki, Effect of grain size on the core loss of nanocrystalline Fe₈₆B₁₃Cu₁ prepared by ultra-rapid annealing, *AIP Adv.* **13**, 025304 (2023).
- [16] G. Bertotti, Space-time correlation properties of the magnetization process and eddy current losses: Theory, *J. Appl. Phys.* **54**, 5293 (1983).
- [17] G. Bertotti, General properties of power losses in soft ferromagnetic materials, *IEEE Trans. Magn.* **24**, 621 (1988).

- [18] K. Suzuki, A. Makino, A. Inoue, and T. Masumoto, Low core losses of nanocrystalline Fe–M–B ($M = \text{Zr, Hf, or Nb}$) alloys, *J. Appl. Phys.* **74**, 3316 (1993).
- [19] K. Inomata, M. Hasegawa, T. Kobayashi, and T. Sawa, Magnetostriction and magnetic core loss at high frequency in amorphous Fe–Nb–Si–B alloys, *J. Appl. Phys.* **54**, 6553 (1983).
- [20] H. Tsukahara, H. Imamura, C. Mitsumata, K. Suzuki, and K. Ono, Role of magnetostriction on power losses in nanocrystalline soft magnets, *NPG Asia Mater.* **14**, 44 (2022).
- [21] Z. Li and S. Zhang, Domain-wall dynamics driven by adiabatic spin-transfer torques, *Phys. Rev. B* **70**, 024417 (2004).
- [22] S. S. Parkin, M. Hayashi, and L. Thomas, Magnetic domain-wall racetrack memory, *Science* **320**, 190 (2008).
- [23] I. L. Kindiak, P. N. Skirdkov, K. A. Tikhomirova, K. A. Zvezdin, E. G. Ekomasov, and A. K. Zvezdin, Domain-wall dynamics in a nanostrip with perpendicular magnetic anisotropy induced by perpendicular current injection, *Phys. Rev. B* **103**, 024442 (2021).
- [24] J. P. Garcia, A. Fassatoui, M. Bonfim, J. Vogel, A. Thiaville, and S. Pizzini, Magnetic domain wall dynamics in the precessional regime: Influence of the Dzyaloshinskii-Moriya interaction, *Phys. Rev. B* **104**, 014405 (2021).
- [25] R. Parsons, B. Zang, K. Onodera, H. Kishimoto, T. Shoji, A. Kato, and K. Suzuki, Core loss of ultra-rapidly annealed Fe-rich nanocrystalline soft magnetic alloys, *J. Magn. Magn. Mater.* **476**, 142 (2019).
- [26] R. Parsons, Z. Li, and K. Suzuki, Nanocrystalline soft magnetic materials with a saturation magnetization greater than 2T, *J. Magn. Magn. Mater.* **485**, 180 (2019).
- [27] R. Parsons, K. Onodera, H. Kishimoto, T. Shoji, A. Kato, and K. Suzuki, Effect of tensile stress during ultra-rapid annealing on the soft magnetic properties of Fe–B based nanocrystalline alloys, *J. Alloy. Compd.* **924**, 166374 (2022).
- [28] R. Parsons and K. Suzuki, Nanocrystalline soft magnetic materials produced by continuous ultra-rapid annealing (CURA), *AIP Adv.* **12**, 035316 (2022).
- [29] K. Suzuki, R. Parsons, B. Zang, K. Onodera, H. Kishimoto, T. Shoji, and A. Kato, Nanocrystalline soft magnetic materials from binary alloy precursors with high saturation magnetization, *AIP Adv.* **9**, 035311 (2019).
- [30] S. Ito, K. Aso, Y. Makino, and S. Uedaira, Magnetostriction and magnetization of iron-based amorphous alloys, *Appl. Phys. Lett.* **37**, 665 (1980).
- [31] K. Narita, J. Yamaguchi, and H. Fukunaga, Saturation magnetostriction and its annealing behavior of $\text{Fe}_{100-x}\text{B}_x$ and $\text{Co}_{100-x}\text{B}_x$ amorphous alloys, *J. Appl. Phys.* **50**, 7591 (1979).
- [32] T. Jagielinski, Magnetostriction and magnetoelastic effects in certain amorphous alloys, *IEEE Trans. Magn.* **17**, 2825 (1981).
- [33] G. Herzer, Magnetization process in nanocrystalline ferromagnets, *Mater. Sci. Eng., A* **133**, 1 (1991).
- [34] F. Fiorillo and C. Beatrice, Energy losses in soft magnets from DC to radiofrequencies: Theory and experiment, *J Supercond. Nov. Magn.* **24**, 559 (2011).
- [35] S. Flohrer, N. Schäfer, J. McCord, S. Roth, L. Schultz, and G. Herzer, Magnetization loss and domain refinement in nanocrystalline tape wound cores, *Acta Mater.* **54**, 3253 (2006).
- [36] K. Suzuki, N. Ito, J. S. Garitaonandia, J. D. Cashion, and G. Herzer, Local random magnetocrystalline and macroscopic induced anisotropies in magnetic nanostructures, *J. Non-Cryst. Solids* **354**, 5089 (2008).
- [37] F. Fiorillo, E. Ferrara, M. Coisson, C. Beatrice, and N. Banu, Magnetic properties of soft ferrites and amorphous ribbons up to radiofrequencies, *J. Magn. Mag. Mater.* **322**, 1497 (2010).
- [38] W. K. Peria, X. Wang, H. Yu, S. Lee, I. Takeuchi, and P. A. Crowell, Magnetoelastic Gilbert damping in magnetostrictive $\text{Fe}_{0.7}\text{Ga}_{0.3}$ thin films, *Phys. Rev. B* **103**, L220403 (2021).
- [39] C. Vittoria, S. D. Yoon, and A. Widom, Relaxation mechanism for ordered magnetic materials, *Phys. Rev. B* **81**, 014412 (2010).
- [40] See Supplemental Material <http://link.aps.org/supplemental/10.1103/PhysRevB.109.104408> for animated simulation results.
- [41] D. Honecker, C. D. Dewhurst, K. Suzuki, S. Erokhin, and A. Michels, Analysis of magnetic neutron-scattering data of two-phase ferromagnets, *Phys. Rev. B* **88**, 094428 (2013).
- [42] K. Suzuki, N. Ito, J. S. Garitaonandia, and J. D. Cashion, High saturation magnetization and soft magnetic properties of nanocrystalline $(\text{Fe, Co})_{90}\text{Zr}_7\text{B}_3$ alloys annealed under a rotating magnetic field, *J. Appl. Phys.* **99**, 08F114 (2006).
- [43] G. G. Savenkov and Y. I. Meshcheryakov, Structural viscosity of solids, *Combust. Explos. Shock Waves (Engl. Transl.)* **38**, 352 (2002).
- [44] G. Herzer, *Handbook of Magnetism and Advanced Magnetic Materials, Novel Materials* (Wiley, New York, 2007), Vol. 4, p. 1882.